Journal of Marine Research, 67, 305–322, 2009

Deep cyclogenesis by synoptic eddies interacting with a seamount

by Andrew D. Greene[1,2], Georgi G. Sutyrin[1], and D. Randolph Watts[1]

ABSTRACT

Strong deep eddies with cyclonic vorticity greater than $0.2\,f_0$ were detected using an array of bottom current and pressure measurements in the Kuroshio Extension System Study (KESS) in 2004–2006. Daily maps showed these deep eddies developed locally. As in the Gulf Stream, meandering of the upper baroclinic jet generates deep cyclones and anticyclones by stretching and squashing the lower water column. However, unlike the Gulf Stream, the smaller vertical stretching and greater water depth in the Kuroshio Extension limits the relative vorticity generated by this vertical coupling process to about $0.1\,f_0$. In the deep Kuroshio Extension the strong cases of vorticity generation and cyclone development are related to stretching driven when water columns are advected off isolated seamounts in the region. The large observed values of relative vorticity are consistent with a straightforward calculation of deep layer potential vorticity conservation.

A barotropic model is used to illustrate the topographic generation of cyclones by ambient currents in synoptic eddies. Positive potential vorticity filaments also develop during the cyclogenetic process with width $L_R = O(20$ km), where L_R is the topographic Rhines scale, and travel anticyclonically around the seamount. Observational evidence lends support to the existence of submesoscale filaments, insomuch as current meter records near the flanks of seamounts exhibited bursts of eddy kinetic energy when bandpass-filtered between the inertial period and eight days.

1. Introduction

Synoptic eddies in the abyss are common in the ocean, especially beneath meandering western boundary currents (Shay *et al.*, 1995; Watts *et al.*, 1995). Here we present data from the Kuroshio Extension System Study (KESS) array. Recent analyses indicate highly variable deep velocities (> 25 cm s^{-1}) and relative vorticities $O(0.2\,f_0)$ which, unlike deep cyclones in the Gulf Stream, cannot be explained alone by stretching effects caused by the main thermocline meandering nor by currents crossing large scale topography. Moveover, the deep barotropic portion of the jet below the Kuroshio Extension is only 5 cm s^{-1}, which is too weak to generate such strong deep eddy variability (> 25 cm s^{-1}) by simple meandering or barotropic instability processes. Therefore we search for other sources of deep flow variability.

1. Graduate School of Oceanography, University of Rhode Island, Narragansett, Rhode Island, 02882, U.S.A.
2. Corresponding author. ***email: agreene@gso.uri.edu***

Besides the local generation of strong deep eddies, remotely generated eddies passed through the Kuroshio Extension region. High and low pressure centers repeatedly propagated into the region from the east with diameters typically 250 km and relative vorticities $< 0.1\,f_0$, i.e., larger and weaker than the strong cases of locally generated cyclones. As they drifted through the array, they encountered the upper Kuroshio Extension jet, rings, and topography. Of these interactions the one that can consistently generate $O(20\%)$ vertical stretching is the interaction of the deep flow with seamounts.

The sea floor in the Kuroshio Extension region has a gentle trend downward toward the southeast from 5300–6400 m. Several seamounts in this region rise above this broad slope (Fig. 1). The height of the seamounts above the local bathymetry is 800–2000 m with radii of 50–75 km. The strongest deep cyclonic eddies were detected offset from a seamount by 100 km or less. Therefore, we investigate the interaction of the deep flow with the local seamounts.

Topographically-induced anticyclonic circulation is commonly observed over the seamounts (Genin *et al.*, 1989). Previous studies suggest that background currents and ambient eddy variability govern the topographic interactions. One explanation of seamount-trapped flows relies on the Taylor-Proudman theorem: an isolated obstacle diverts flow in a rotating fluid around an isolated seamount and generates a column of trapped circulation (Greenspan, 1968; Hopfinger and Van Heijst, 1993). More formal explanations of

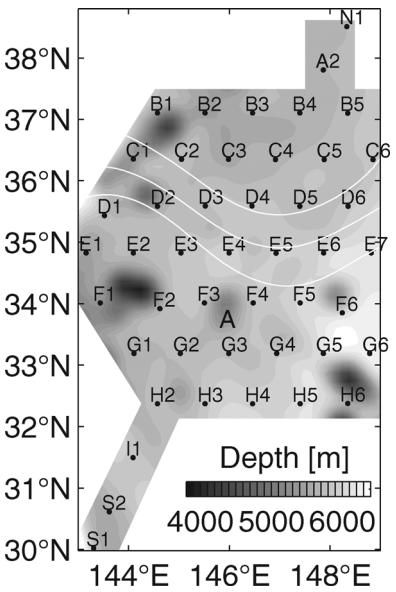

Figure 1. Topography in the KESS region is shown with gray-shaded contours. Topography has been smoothed with a low-pass wavenumber filter with a 80 km cutoff. The solid white contour lines indicate the mean position of Kuroshio Extension jet axis and its northern and southern boundaries. Superimposed are the locations of the CPIES instruments.

anticyclones over topography are provided by equilibrium statistical mechanics (Merryfield *et al*., 2001; Nycander and LaCasce, 2004).

The initial value problem for uniform flow incident on a small amplitude seamount has been investigated earlier numerically in a number of barotropic and stratified models. Using a three-dimensional model with nine levels and periodic boundary conditions, Huppert and Bryan (1976) found that starting from rest, the evolution of the flow redistributes vorticity in such a way that anticyclonic vorticity remains over the topographic feature, while water shed from the seamount induces a cyclonic vorticity anomaly. For sufficiently strong incident flow, the shed fluid is advected downstream forming a cyclonic eddy. If the incident flow is relatively weak, interaction between anticyclonic and cyclonic vorticity patterns traps the cyclonic eddy and the eddy remains in the vicinity of the topographic feature.

They interpreted their results by using simple analytical calculations based on an approximate representation of their streamfunction in terms of line vortices, and suggested that observations by Vastano and Warren (1976) of an eddy in the vicinity of the Atlantis II Seamount and existence of the large amount of high frequency energy near the bottom of the ocean measured by the MODE experiment may be partly explained in terms of this mechanism of topographic cyclogenesis. The different typical responses of a uniform flow impinging on an isolated seamount were synthesized using barotropic models with downstream boundary conditions which allowed vorticity to be advected smoothly out of the domain (James, 1980; Verron and Le Provost, 1985). Similar results were obtained for a two-layer contour dynamical model for a tall seamount penetrating the upper layer (Thompson, 1993).

Generally, unsteady flow over a sloping bottom is known to produce a bottom-intensified mean flow with a correlation between streamfunction and topography and anticyclonic motion over bumps (Dewar, 1998). In contrast, upper layer variability can produce surface-intensified topographic circulation over a tall seamount (Sutyrin, 2006). Such rectified flows are related to potential vorticity stirring which becomes strongly anisotropic over steep slopes where topographic Rossby waves prevent the flow from achieving the scale of the topography. This may lead to the formation of alternating jets with spatial scale about 20 km or less, estimated from the topographic Rhines scale $L_R = (UH/sf)^{1/2}$, with typical eddy velocity $U \simeq 0.1$ m s^{-1}, ocean depth $H \simeq 4$ km, and topographic slope $s \simeq 10^{-2}$ (Vallis and Maltrud, 1993). For a uniform background potential vorticity gradient, lateral mixing of potential vorticity across the background gradient tends to be inhomogeneous and leads to staircases, which Dritschel and McIntyre (2008) argue is why persistent jets are commonplace in planetary atmospheres and oceans and why such jets tend to sharpen themselves when disturbed. Our observations in the Kuroshio Extension and these previous studies motivated us to consider what kind of variability can be generated by time-varying currents passing an isolated seamount.

The Synoptic Ocean Prediction Experiment (SYNOP) was the first field experiment that clearly demonstrated the deep-flow fields beneath the Gulf Stream were organized into coherent vortices. SYNOP revealed that deep cyclones developed and intensified jointly with

large amplitude Gulf Stream meander troughs. Case studies of steep meander events revealed that the production of positive relative vorticity in the deep ocean could be accounted for by the local meander-induced stretching of the lower water column (Savidge and Bane, 1999a,b; Howden, 2000).

In 2004 the multi-institutional collaborative project KESS was launched. One of the goals of KESS has been to understand the processes coupling the baroclinic and barotropic circulation. One working hypothesis was that meandering of the Kuroshio Extension couples the baroclinic front to deep eddies, via baroclinic instability, which in turn steer the baroclinic front. While this holds true for a number of events in the near neighborhood of the baroclinic front, there are additional cases away from the baroclinic front in which a seemingly spontaneous spin-up of a deep cyclone occurs without the baroclinic stretching produced by jet meandering. Since the array was designed to resolve mesoscale processes, we conducted potential vorticity analyses on the deep layer. All deep eddies generated within the KESS array with vorticity $|\zeta| > .15\, f_0$ in KESS were cyclones.

This paper is focused on deep cyclogenesis due to the influence of isolated seamounts. We will show that the interaction between deep synoptic currents and seamounts can produce detached cyclones. Since mesoscale observational arrays can smooth over submesoscale features, we utilize a semi-spectral barotropic model to study the topographically generated cyclones. The rest of the paper is organized as follows. Section 2 describes the observational data. Section 3 shows how we calculate lower layer potential vorticity. Section 4 presents numerical simulations of the barotropic Rossby waves interacting with an isolated seamount. Section 5 provides a discussion and Section 6 offers some conclusions and suggests future work.

2. Observational data

Forty-six Current and Pressure recording Inverted Echo Sounders (CPIES) were deployed in the Kuroshio Extension region, 30–40°N and 140–150°E, during May 2004 –July 2006. Instruments were spaced on average 88 km zonally along lines separated 88 km meridionally, diagonally offset (Fig. 1). The Inverted Echo Sounder (IES) component measures the vertical acoustic travel time (τ) round trip from the sea floor to the surface and back. Variations in τ are mainly due to changes in depth of the thermocline. In this study τ is used with historical hydrography to estimate the 6°C isotherm depth Z_6, which in turn is used as a proxy for the base of thermocline. This method has been utilized with success in the North Atlantic Current (Meinen and Watts, 2000), Subantarctic Front south of Tasmania (Watts *et al.*, 2001), and the Gulf of Mexico (Donohue *et al.*, 2006).

Each IES was equipped with a pressure sensor (PIES) to measure deep pressure variations (p), the barotropic signal. Thirty-seven PIESs also had an Aanderaa™ Doppler current sensor tethered 50 m above the bottom (CPIES). Sampling intervals for τ, p, u, and v were hourly, where u and v are the zonal and meridional velocities measured by the current sensor. In addition, there were seven deep moorings with RCM-11 current meters, sampling at 2000

m, 3500 m, and 5000 m, deployed across the Kuroshio Extension. All the data from the KESS array were low-pass filtered using a fourth order Butterworth filter with a three day cutoff period. This effectively removes the effects of the major tidal constituents, inertial oscillations, and surface waves while retaining the low-frequency mesoscale variability. Transients in the time series were reduced by chopping off 1 day (1/3 of the filtering period) at the beginning and end of each time series. Data gaps were filled by linear interpolation, so filtering could be carried out. Direct comparisons of CPIES estimated temperatures and velocities to measurements by the current meter moorings in the KESS array show good agreement (Donohue *et al.*, 2009).

Deep pressure and current measurements were used to generate optimally interpolated[3] (OI) daily maps of velocity, streamfunction, and relative vorticity ζ at 5300 m. Optimal interpolation was also utilized for mapping Z_6.

CPIES that were deployed close to the flanks of seamounts recorded bursts of strong rectilinear currents with periods shorter than the ambient mesoscale variability. We believe these currents are associated with the topography and are highly localized, therefore they were not used in our OI mapping which maps horizontally nondivergent flow fields. But the individual current records will be used to provide evidence of filaments and submesoscale activity.

3. PV structure from KESS

The mapped ζ fields revealed deep eddies with relative vorticity ζ values exceeding $0.20 f_0$, where f_0 is calculated at 35°N, near the center of our array. Under the assumption that layered potential vorticity (PV) is conserved, and if initially the deep $\zeta \approx 0$, then the elevated relative vorticity in an eddy would have required a lower layer stretching of 20%. However, the ocean is so deep in the KESS region, 5300–6400 m, that vertical excursions of the thermocline $\approx$ 500 m can only cause a 10–12% change in the lower layer thickness, with matching size (ζ/f_o). Moreover, observations demonstrated that these strong deep eddies developed with little to no baroclinic stretching. This quantifies the statement in the Introduction that the observed values of ζ cannot be explained by meandering of the baroclinic jet.

We define the lower layer as the portion of the water column confined between the base of the thermocline and the ocean bottom. Variations in Z_6 represent vertical excursions of the base of the thermocline. Z_6 deepens 500–600 m across the Kuroshio Extension jet from north to south, and does not outcrop to the north. Lower layer thickness is $H = Z - Z_6$ and on average H is 5000 m, where Z is the bathymetry, version 8.2 (Smith and Sandwell, 1997), shown in Figure 1. Direct velocity measurements beneath the thermocline confirmed

3. Optimal interpolation is an objective analysis scheme used for data interpolation and mapping (Bretherton *et al.*, 1976). The optimally interpolated map minimizes the error between the estimate and the measurement and through the correlation functions enforces horizontal nondivergence. A Gaussian spatial correlation function was fitted to the data for τ and for p. The empirically derived correlation length scale for τ is 130 km (75 km) for temporal scales greater (less) than 60 days. The correlation length scale for deep pressures is 100 km.

that deep vertical shear is weak. Between 2000 m and 5000 m the mean speeds differ by less than 0.3 cm s^{-1}, therefore we treat the lower layers as barotropic in our PV calculations. The lower layer potential vorticity was calculated as

$$\mathrm{PV} = \frac{\zeta + f}{H} \tag{1}$$

where f is the planetary vorticity.

a. A case study and a puzzle

Daily maps of PV and pressure were generated to illustrate how deep barotropic eddies are generated by seamounts. Figure 2 illustrates the generation of a deep cyclonic vortex, where the colors are lower layer potential vorticity, the deep pressure field is represented by the black (low pressure) and grey (high pressure) contour lines, and the blue lines denote Z_6 at 300 m, 500 m, and 700 m, respectively from north to south side of the Kuroshio Extension. Between yearday 333–339 an intense low pressure center develops near 33°N, 146°E. The cyclone had a pressure anomaly –0.24 dbar ($\approx$ –24 cm) at the center and maximum swirl speeds exceeding 31 cm s^{-1}. At its most southern position, 33°N, the cyclone had a value of ζ equal to (0.18 to 0.21) f_o, where 0.03 f_o range in vorticity is the uncertainty estimate from OI mapped relative vorticity in the KESS array for a circular eddy with e-folding radius $R_L = 80$ km. Uncertainties in mapped pressure and vorticity are discussed in Section 5a. Noteworthy is that during the days leading up to the deep eddy spin-up the observed baroclinic stretching was far too small to have produced the observed deep relative vorticity. This apparent (but unlikely) spontaneous spinup of a deep cyclone motivated us to investigate the effects of topographic stretching on vorticity generation.

The potential vorticity field depicts a different story of cyclone generation than do the bottom pressure maps alone. In Figure 2 the PV field has initially a high anomaly centered on a 700 m tall seamount at 34 °N 145.9°E, labeled "A" in Figure 1. The ambient incident currents are shown in Figure 3 and we can estimate their Rossby numbers using the radius of the seamount (50 km). For the first 5.5 months of this record the current speed was 3 cm/s, with Rossby number $R_o = 0.007$. From yearday 320–350 they increased to 14 cm/s, with $R_o = 0.034$, flowing generally southward. In Figure 2 the PV anomaly migrated southward off the seamount between yeardays 334-to-338 and by yearday 338 the amplitude of the PV anomaly arose almost entirely from the cyclonic vorticity in the newly formed eddy. The sequence of PV maps in Figure 2 suggests that the vorticity for the cyclone may have originated at seamount "A," where the deep water column could have acquired so much stretching vorticity.

4. Modeling the interaction of synoptic eddies with a seamount

The observations suggest the cyclone formation was a result of water column stretching as the PV anomaly migrated off the seamount. In this section we utilize a barotropic model

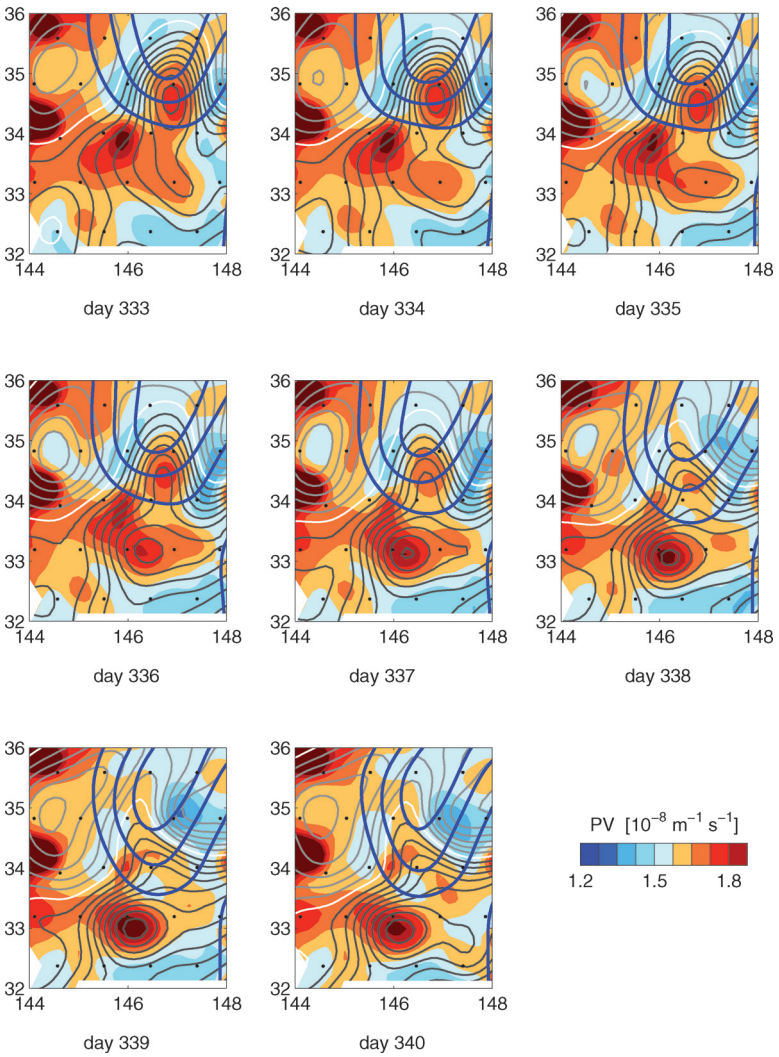

Figure 2. Daily maps of lower layer potential vorticity (colorbar at middle range is approximately f_0/H_0). The deep pressure anomaly field is superimposed in solid grey (positive anomaly) and black (negative anomaly) contours (CI = 0.025 dbar). Three bold blue contours denote the 300 m, 500 m, and 700 m depth of the 6°C isotherm, with the northernmost contour representing the 300 m isoline. The upper jet path had a steep trough at 146–147°E during this interval, because the first crest at 144–145°E had shifted north of its mean position. The baroclinic structure remains separated to the north of the strong cyclogenesis event near 33°N 146°E.

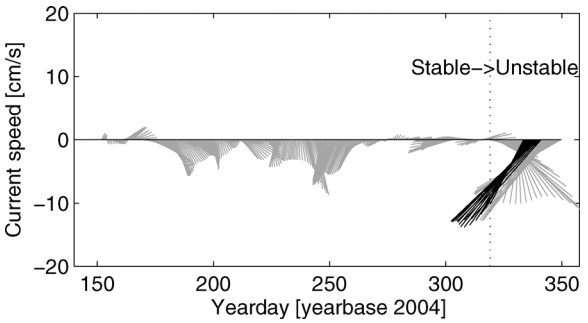

Figure 3. Semi-daily currents incident upon seamount "A" averaged from the center out to a radius of 80 km. The black vectors denote the time period in which the case study (Section 3) was performed. The vertical dotted line at yearday 320 is at the start of the strong deep synoptic currents. The strengthening of deep currents coincides approximately with a regime shift from stable to unstable meandering in the upper Kuroshio jet.

for the purpose of qualitatively illustrating the cyclone generation process in the deep ocean. The intention of the model is to gain physical insight into our KESS observations but it does not attempt to reproduce them.

a. The barotropic model equations

We consider a barotropic flow in a rotating fluid with a rigid-lid on the β-plane with topography. The lower layer in KESS is barotropic and its thickness can change due to vertical thermocline excursions or topography, and since we are concerned with the effects of the latter, a rigid-lid approximation is used to isolate the effects of topographic stretching. The model uses the quasi-geostrophic vorticity equation

$$\partial_T \nabla^2 \Psi + J(\Psi, Q) = D, \qquad Q = \nabla^2 \Psi + \beta Y + \frac{f_0}{H_0} H(X, Y), \tag{2}$$

where Ψ is the streamfunction and J denotes the Jacobian: $J(F, G) \equiv \partial_X F \partial_Y G - \partial_Y F \partial_X G$, β is the meridional gradient of the Coriolis parameter f about a central value f_0, H_0 is the mean ocean depth, and H is the bottom topography. When the dissipation term $D = 0$, this equation describes the Lagrangian conservation of potential vorticity, Q.

Choosing the length scale L, and the time scale, T_0, we introduce nondimensional coordinates $(x,\ y) = (X/L, Y/L)$, time $t = T/T_0$, the streamfunction $\psi = \Psi T_0/L^2$, and potential vorticity $q = QT_0$, so that the basic equation becomes

$$\partial_t \nabla^2 \psi + J(\psi, q) = DT_0^2, \qquad q = \nabla^2 \psi + \epsilon y + h(x, y), \tag{3}$$

where $\epsilon = \beta L T_0,\ h = f_0 T_0 H/H_0$.

The synoptic eddies are prescribed by a westward propagating doubly-periodic Rossby wave

$$\psi_W = a\left[\sin\left(kx + \frac{\epsilon k t}{k^2+m^2}\right)\right]\cos(my),$$

where k and m are zonal and meridional wavenumbers and a is the wave amplitude. This is an exact solution of (3) for flat bottom frictionless flow, $h = 0$, $D = 0$. In the presence of topography, we include bottom friction and small-scale dissipation acting on the vorticity deviation from the prescribed Rossby wave

$$DT_0^2 = -(E + A\nabla^4)\nabla^2(\psi - \psi_W).$$

Here the bottom friction $E = f_0 T_0 h_E/2H_0$ is proportional to the boundary layer thickness h_E, and A is the coefficient of hyperviscosity which is kept to a minimum avoiding enstrophy accumulation at small scales.

b. Numerical setup

A biperiodic pseudo-spectral code is used to model the finite time, fully nonlinear evolution of this interaction on a beta-plane. The initial conditions at $t = 0$ are $\psi = \psi_W$ over the whole domain. A Gaussian circular seamount $h(r) = h_0 \exp(-(r/r_0)^2)$ is prescribed at the center of the domain: $r^2 = x^2 + y^2$. High horizontal resolution is used (256 nodes in each direction).

Without the seamount, such a Rossby wave drifts steadily westward with speed $\epsilon/(k^2 + m^2)$, and the characteristic time scale of its instability to reorganize into zonal jets is much larger than the period of propagation $2\pi(k^2 + m^2)/\epsilon k \approx 250$ for $k = m = 2$ and the beta-parameter $\epsilon = 0.1$. Other nondimensional parameters are the seamount height h_0, radius r_0, maximum velocity in the synoptic field $2a$, and bottom friction E.

In the numerical setup, the nondimensional domain size is 2π and the distance between the streamfunction extrema is π/k, which characterize the diameter of synoptic eddies. To interpret the results in dimensional form, we may select $L = 160$ km which is a typical deep eddy diameter in KESS. $L = 160$ km corresponds to a domain size of about 1000 km, approximately the same as the KESS domain. Then the time scale is defined by the beta-parameter: $T_0 = \epsilon/\beta L \approx 3 \cdot 10^4$ s, and the velocity scale $L/T_0 \approx 5$ m s^{-1}, that gives the velocity on the order of 0.1 m s^{-1} for typical value $a = 0.01$ and $k = 2$. The topography amplitude is characterized by $h_0/f_0 T_0 \approx h_0/3 = 1/7$ for the typical value $h_0 = 0.4$ and $f_0 = 10^{-4}$ s^{-1}.

c. Results of simulations

A simulation for a narrow seamount with $h_0 = 0.4, r_0 = 0.19, a = 0.01, E = 0, A = 10^{-9}$ is shown in Figure 4. In dimensional form, h_0 and r_0 are similar in height and e-folding radius to seamount "A." For completeness we have included model runs in which both the anticylonic (Fig. 4, top row) and cyclonic (Fig. 4, bottom row) parts of the wave

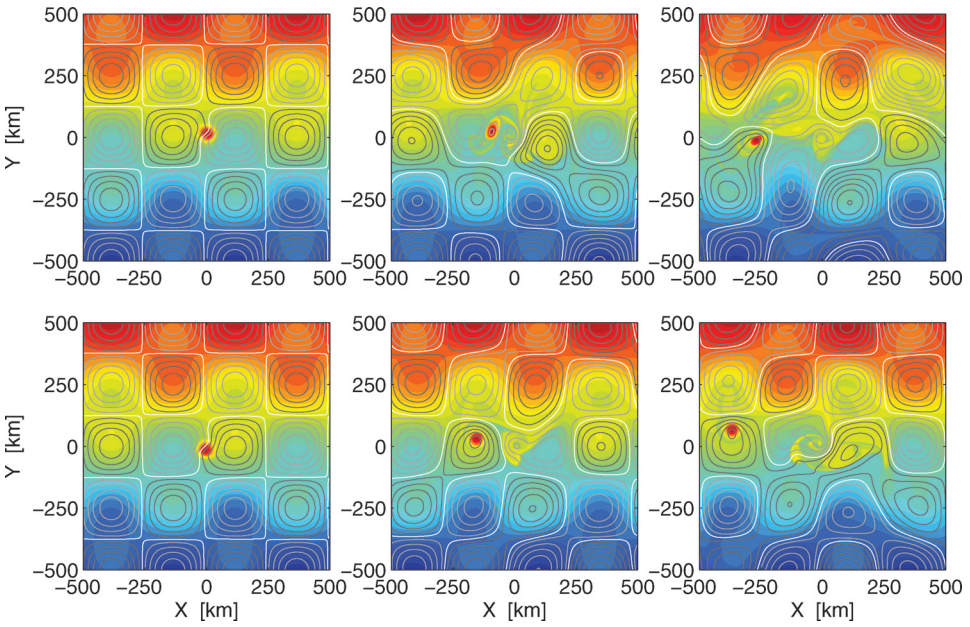

Figure 4. Quasi-geostrophic potential vorticity field from the barotropic model. Top row (bottom row) shows the cyclogenesis process for the case when the anticyclonic (cyclonic) part of the Rossby wave field is incident upon the seamount. Left, middle, and right panels show respectively elapsed time 0, 0.5, 1 period of the synoptic Rossby wave field with color-shaded contours, with yellow and red colors indicating high PV. Grey and black contours denote the streamfunction, where grey (black) indicates anticyclonic (cyclonic) circulation and the zero streamline between them has a solid white contour. Seamount at (0,0) km. The cyclonic feature near (−280, 0) km in the top row or (−360, 0) km in the bottom row started as a large PV anomaly that separated from the seamount and formed a cyclone.

field are incident upon the seamount. Since, the results of both simulations are quite similar, the following discussion deals with the cyclogenetic process with an incident anticyclonic Rossby wave. The potential vorticity q field with superimposed streamfunction, solid grey contours for positive (anticyclonic) values and black contours for negative (cyclonic) values, are shown in Figure 4 at time $t = 0$ (left panel), and after one-half and one wave period of the incident Rossby wave in, respectively, the middle and right panels. After 1/2-wave period a cyclonic feature has detached west of the seamount. There is also an anticyclone above the seamount with small scale spirals of vorticity wrapping around the seamount. After the cylone is formed it continues to translate westward (right panel). Figure 5 shows a zonal section through the seamount center: the initial q peak over the seamount (solid black line) with periodic Rossby wave; and after one Rossby period T_R the q amplitude is smaller (dashed black line), corresponding to negative (anticyclonic) vorticity over the seamount (grey line), while a positive PV and relative vorticity peak west of the seamount corresponds to the cyclonic eddy seen in Figure 4.

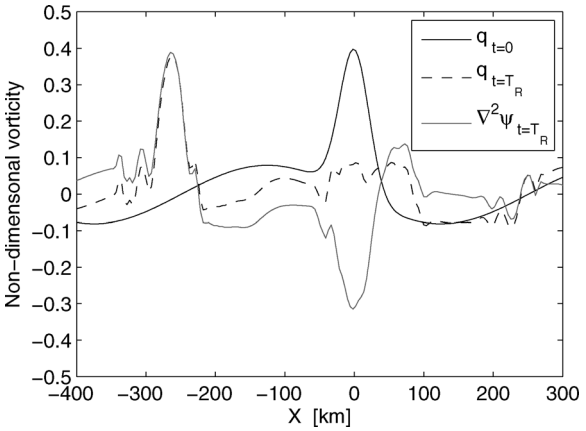

Figure 5. Zonal section of nondimensional vorticity. The solid and dashed black lines represent the potential vorticity initially ($t = 0$) and after one Rossby wave period ($t = T_R$). Solid grey line denotes the relative vorticity anomaly after one Rossby wave period. The positive PV feature at $X =$ –240 to –300 km contains entirely cyclonic vorticity, acquired from stretching as ta PV anomaly was swept off the seamount.

Note that, in order to cause a cyclone to form away from a seamount, currents must be strong enough to advect the water column off the seamount during the synoptic eddy timescale. For example, a run with much weaker incident synoptic eddies with $a = 0.002$, produced cyclonic filaments that remained attached to the seamount (not shown). The actual threshold for detachment may also depend on the seamount parameters and friction parameters chosen.

5. Discussion

a. KESS observations

The observed spin-up of the deep cyclone in our case study (Section 3) had cyclonic vorticity consistent with topographic stretching of the lower layer. Referring back to Figure 2, the lower layer thickness atop seamount "A" was $H_1 = 5080 - 860$ m $= 4220$ m with planetary vorticity f_1 and after the PV anomaly left the seamount the thickness was $H_2 = 5810 - 930$ m $= 4880$ m with planetary vorticity f_2. Under the assumption that there was zero initial relative vorticity atop the seamount, stretching should generate relative vorticity

$$\zeta = f_1 \frac{H_2}{H_1} - f_2 = (.17 \pm .02) f_0. \tag{4}$$

The uncertainly of $0.02 f_o$ in relative vorticity arises from uncertainty (≈ 50 m) in estimating Z_6. This calculation of ζ agrees well with our observed relative vorticity (0.18 to 0.21) f_0.

Assuming the initial relative vorticity is zero atop the seamount is arguably valid because the incident synoptic currents (Fig. 3) had been much weaker for at least the preceding 5.5 months. Thus the water above the seamount had likely been trapped in a Taylor column for long enough that its relative vorticity would have decayed by friction. Our daily maps of bottom PV, although the input measurements could have missed localized small-scale relative vorticity atop the seamount, indicate that the PV anomaly discussed in Section 3a and Figure 2 remained atop the seamount for the preceding 5.5 months. Nevertheless, we must bear in mind that the array had been designed to sample the synoptic currents rather than adequately resolve the likely smaller-scale current structure atop the seamounts. So caution must be taken when estimating from our measurements the vorticity atop a seamount.

We conducted a simulation of analytic eddies with various Gaussian e-folding radii R_L in order to determine how well the KESS array detects and estimates their amplitudes. The results were as follows. The KESS array spacing and the OI mapping procedures allow for the detection of eddies with the correct sign (cyclone or anticyclone) even for the smallest simulated size $R_L = 15$ km. For eddies with $R_L = 50$ km, the OI mapped fields recover 80% and 50% of the respective amplitudes of the true pressure and vorticity values. The corresponding numbers for eddies with R_L = 80 km are respectively 95% and 85% of the true pressure and vorticity values.

Returning to Figure 2, we can show that R_L of the eddy is approximately 80 km and is not artificially large due to the sampling and OI mapping. Recall that deep current meters as well as pressure sensors measure at each site. The vorticity ζ_0 and pressure p_0 at the center of a Gaussian shaped eddy are related as $\zeta_0 = -(4/f\rho_0)(p_0/{R_L}^2)$, where $\rho_0 = 1050\,\mathrm{kg/m^3}$ is the average deep density. The mapped values on day 339 are $\zeta_0 = 0.18\,f_0$ and $p_0 = -0.24$ dbar. A Gaussian fit to the eddy pressure field resulted in a 80 km e-folding scale, R_L. A mapped R_L = 80 km is consistent with $(4p_0/\zeta_0 f\rho_0)^{1/2} \approx 85$ km. The counterargument is that if a PV-conserving feature (with $\zeta_0 = 0.18\,f_0$, as mapped) had a smaller eddy radius, say 60 km, then the central pressure would be correspondingly diminished by the ratio $(60/80)^2$ to 0.14 dbar, which is far below the uncertainty limits of the observed central pressure. Thus given the mapped extrema for ζ_0 and p_0, the radius cannot be much smaller than 80 km, and with a radius of 80 km the mapped estimates of ζ and p are (for the KESS array) respectively at least 85% and 95% of the true values. Moreover using $R_L = 80$ km, the small fluctuations in mapped PV (one contour interval) during days 336–337 can be explained by our estimated mapping uncertainty (underestimate) of ζ $(0.03\,f_0)$ for an eddy of this scale.

b. Advection of cyclones by the synoptic field

The Kuroshio Extension is known to oscillate between stable and unstable states on decadal time scales (Qiu and Chen, 2005). The stable (unstable) state is characterized by low (high) eddy kinetic energy, weak (strong) meandering of the jet, and a shorter (longer) jet path length. During the first six months of the KESS deployment, the Kuroshio Extension

was in a stable state, followed by an unstable state thereafter. Throughout the first six months the observed bottom currents remained weak (Fig. 3), 3 cm s^{-1} on average, near seamount "A" and a high PV anomaly remained atop it. In late November the Kuroshio Extension underwent a transition to an unstable state in which the mean bottom currents increased to 14 cm s^{-1}. We attribute the migration of the PV anomaly off seamount "A" to the increased local bottom currents.

This interpretation agrees with the findings of Huppert and Bryan (1976). They found that cyclones could be advected off a topographic feature if sufficiently strong flow was present. If the flow was too weak, the interaction between cyclonic and anticyclonic vorticities trapped the cyclone in the vicinity of the topographic bump.

It is also useful to compare our results with earlier studies of the initial value problem in a barotropic model with steady and spatially uniform incident flow, where the most important nondimensional parameter was found to be the ratio of topographic stretching to the Rossby number

$$S = \frac{\Delta H L f_0}{H_0 U} \equiv \frac{\frac{\Delta H}{H_0}}{R_o}$$

where ΔH is the topographic height, U is the flow velocity, and L is the seamount radius. When $S < S_{cr}$, the cyclonic vortex separates from the seamount and is advected downstream, while for $S > S_{cr}$ the cyclonic vortex is trapped in the vicinity of the topographic feature and is strongly deformed due to interaction with the topographic anticyclone. $S_{cr} = 11$ according to results by Verron and Le Provost (1985) for the f-plane. The same value of S_{cr} is obtained from the Huppert and Bryan (1976) result if you take the limit as stratification goes to zero; i.e., homogeneous flow. Another way to interpret the above criteria is that if $R_o > 0.09\Delta H/H_0$, then a cyclone will separate from the seamount. Estimates of S from the observed currents in Figure 3 before and after yearday 320 are $S = 19.5$ and $S = 4$, respectively. Hence the low and high incident currents bracket the criterion for S set forth by Verron and Le Provost (1985). It is noteworthy that the findings of Verron and Le Provost (1985) were based on a steady uniform flow over a circular seamount, whereas the deep currents in KESS vary in space and time.

c. KESS vs Gulf Stream Cyclones

Unlike the abyssal cyclones in the Gulf Stream Extension observed during SYNOP (Watts *et al.*, 1995), in which vertical stretching of the bottom layer by meandering of the upper baroclinic jet generated the deep eddies, the eddies we focus upon in this paper are not generated via baroclinic stretching. In fact, during the growth of the cyclone in the case study the thermocline slightly squashed the lower layer thus slightly counteracting the strong cyclogenesis.

In general, the Gulf Stream eddies were longer lived (4–6 vs. 2–3 weeks) and had greater swirl speeds (30–40 vs. 25–30 cm s^{-1}) (Savidge and Bane, 1999a). The radius of maximum

velocity for Gulf Stream eddies was 55 km and in the Kuroshio Extension it is 45 km, in addition the radius in which eddy swirl speeds could be distinguished from ambient background flow was larger in the Gulf Stream. While the spatial and velocity scales are different, the observed values of relative vorticity are similar $O(0.2 f_0)$. This is easily seen because the ratio of the maximum swirl speeds to radius of maximum speed in each case is comparable.

d. Evidence of submesoscale filaments

The model simulations revealed the important role that submesoscale dynamics may play in the evolution of the potential vorticity field near a seamount. During the cyclogenetic process in the model high potential vorticity filaments of $O(L_R \approx 20$ km) width swirled around the seamount. The filaments could also be observed in the vicinity of the detached eddy (Figs. 4 and 5). We therefore sought in our data for supporting evidence of such filaments. The task is difficult because the KESS array could not resolve submesoscale features, but individual current records would of course include whatever variability passed a point. Moveover all the CPIES site locations had been carefully selected to avoid the seamount flanks and minimize direct influence of seamounts.

A simple signature scalar indicator of submesoscale features is eddy kinetic energy (EKE) of the band-pass filtered currents in the band between the inertial period and eight days (Fig. 6). The upper bound of eight days filters out topograhic Rossby waves (TRWs) at all but one CPIES site, B1. TRWs have a minimum period of ten days for alongslope propagation given the deep buoyancy period $\geq$ five days and topographic slope ≤ 0.02. Note that the minimum TRW period at B1 is seven days. The panel third down from the top in Figure 6, site B5, exemplifies records from most sites far removed from seamounts and sites near seamounts but with weak background currents, which displayed little to no energy in the sub-mesoscale band. In contrast site F4, located on the eastern flank of seamount "A," exhibited large bursts of EKE in the latter half of the current record (Fig. 6, top panel). For the first 6 months EKE was weak at F4 and the incident currents at seamount "A" were also weak (Fig. 3). The large bursts of EKE near day 385 correspond to multiple eddy migrations off seamount "A", as seen in our lower layer PV maps (not shown). This is consistent with model results that the high potential vorticity filaments can be swept off the seamount by sufficiently strong incident flow. Large bursts of EKE were also seen, among others, at site F5 which was located on the western flank of a seamount. Typically, sites located near (far away from) seamounts recorded large (small) record-average EKE values in the inertial to eight day time band (Fig. 6, bottom panel).

6. Conclusions

Strong deep cyclones were detected beneath the Kuroshio Extension during KESS. Some eddy features developed and evolved locally and seemingly spontaneously in the daily maps of ζ, with cyclonic vorticities as large as $0.2 f_0$. While lower layer stretching due

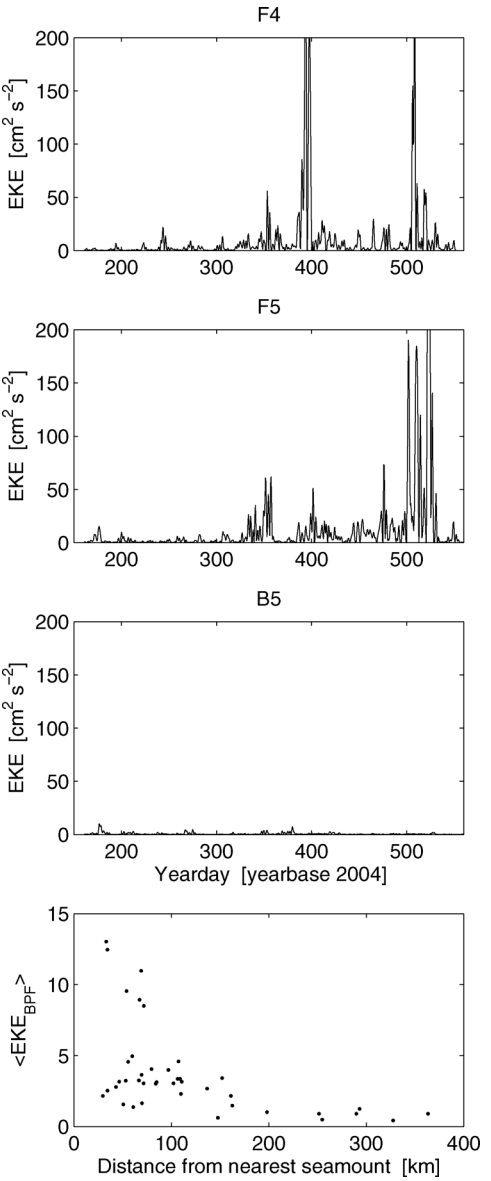

Figure 6. Upper three panels: Eddy kinetic energy at three sites from bottom current measurements bandpass filtered between the inertial period and eight days. We think of this band as submesoscale and suggestive of the presence of small scale variability such as filaments. Site B5 is representative of all KESS CPIES sites that were well-separated from seamounts and had negligible EKE in this band. Sites F4 and F5 were respectively 54 km and 69 km away from a seamount, and their EKE in this band increased starting yearday 350, shortly after the increase in strength of the deep mesoscale currents. Lower panel: Mean EKE, at each site, in the inertial to eight-day time band as a function of distance from the nearest seamount.

to the meandering of the baroclinic jet does account for many observed deep eddies with anticyclonic and cyclonic vorticity, the magnitude of vorticity produced by this process is limited to about $0.10\,f_0$ because the ratio of thermocline depth change to bottom layer thickness is small in the Kuroshio Extension. Moreover, the mean deep jet (< 5 cm s^{-1}) and advection across the gently sloped large scale topography is too weak to account for the development of the most intense observed cyclonic deep eddies.

In Section 3 we presented a case study of a deep cyclone that evolved locally away from the Kuroshio jet. It was among the first of several strong deep cyclones that developed mid-array in KESS, starting when a "stable" interval (the first six months of our observations) transitioned to an energetic interval during the next ten months in which the deep synoptic currents increased by a factor of two to five, which coincided with strong jet meandering. The feature began as an isolated high potential vorticity anomaly located atop a seamount, and we tracked its development as it migrated off the seamount, swept by a sudden increase of incident synoptic currents. The evolution of the deep vorticity field was mapped daily from the mesoscale-resolving array of data from near-bottom current meters, bottom pressure sensors, and acoustic travel times. Independently, simple diagnosis of bottom layer PV conservation estimated the relative vorticity in a water column that had been advected off the seamount onto the surrounding deeper flatter topography (assuming initially zero relative vorticity, as was plausible for the water column having resided relatively undisturbed atop the seamount). The two estimates of ζ agreed within our uncertainty estimates. Altogether, the stretching vorticity created as the PV anomaly swept off the seamount was of correct sign and magnitude and timing and direction of advection to account for the observed spin-up.

Using a barotropic model, we simulated the interaction of incident Rossby waves with an isolated seamount, treated as an initial-value problem. Besides the well-known generation of a topographic anticyclone over the seamount top, an annulus of highly variable cyclonic vorticity was formed, encircling the flanks of the seamount. We suggest this is related to potential vorticity staircases formed due to mixing across the strong potential vorticity gradient over the seamount slope, and the natural scale of features is the topographic Rhines scale. They translate anticyclonically around the seamount resembling topographic waves. The intensity of incident currents of synoptic eddies must be large enough to cause cyclone separation from the seamount. Variable advection in the incident Rossby wave results in repeated separation of these cyclonic filaments. Although the KESS array was not intended to resolve features as small as the filaments, evidence supporting their existence, their timing, and location is presented from the point current meter measurements.

Importantly, the model shows that the initial high potential vorticity anomaly atop the seamount could be advected off of the seamount and transformed into a cyclonic vortex, with a central core of potential vorticity anomaly due almost entirely to cyclonic relative vorticity and as strong as the initial q atop the seamount. This sequence of model events qualitatively resembled - in location, scale, and vorticity magnitude - the strongest cyclogenesis events observed in KESS.

The mechanism in this study for generating strong deep cyclones suggests future study directions. How does the threshold strength for constant incident currents change for non-uniform time-varying flows? What role do submesoscale filaments play in the cyclogenetic process? What governs their ultimate size and lifespan? In particular for the Kuroshio Extension, what are the consequences of these locally generated strong deep eddies? How do they couple with the upper ocean and possibly variably steer the Kuroshio jet? What PV flux divergences do they cause, and how does this affect the recirculation gyre located south of the Kuroshio Extension?

Acknowledgments. We are grateful to the US National Science foundation for supporting this study as part of the Kuroshio Extension System Study (KESS), under NSF grant OCE02-21008. We wish to thank Gerry Chaplin and Erran Sousa and the URI Equipment Development Lab for preparing and deploying the CPIES array. We are particularly grateful to Kathleen Donohue and Karen Tracey for scientific discussions and processing/management of the data.

REFERENCES

Bretherton, F. P., R. E. Davis and C. B. Fandry. 1976. A technique for objective analysis and design of oceanographic experiments applied to MODE-73. Deep Sea Res., *23*, 559–582.

Dewar, W. K. 1998. Topography and barotropic transport control by bottom friction. J. Mar. Res., *56*, 295–328.

Donohue, K., P. Hamilton, K. Leaman, R. Leben, M. Prater, D. R. Watts and E. Waddell. 2006. Exploratory study of deepwater currents in the Gulf of Mexico, Volume II: Technical report. U.S. Dept. of the Interior, Minerals Management Service, Gulf of Mexico OCS Region, New Orleans, LA, OCS Study MMS, 430 pp.

Donohue, K. A., D. R. Watts, K. L. Tracey, A. D. Greene, and M. Kennelly. 2009. Mapping circulation in the Kuroshio Extension with an array of Current and Pressure recording Inverted Echo Sounders. J. Atmos. Oceanic Technol., (in press).

Dritschel, D. G. and M. E. McIntyre. 2008. Multiple Jets as PV Staircases: The Phillips Effect and the resilience of eddy-transport barriers. J. Atmos. Sci., *65*, 855–874.

Genin, A., M. Noble and P. F. Lonsdale. 1989. Tidal currents and anticyclonic motions on two North Pacific seamounts. Deep-Sea Res., *36*, 1803–1815.

Greenspan, H. P. 1968. The Theory of Rotating Fluids, Cambridge University Press, 325 pp.

Hopfinger, E. J. and G. J. F. Van Heijst. 1993. Vortices in rotating fluids. Ann. Rev. Fluid Mech., *25*, 241–289.

Howden, S. D. 2000. The three-dimensional secondary circulation in developing Gulf Stream meanders. J. Phys. Oceanogr., *30*, 888–915.

Huppert, H. E. and K. Bryan. 1976. Topographically generated eddies. Deep-Sea Res., *23*, 655–679.

James, I. N. 1980. The forces due to geostrophic flows over shallow topography. Geophys. Astrophys. Fluid Dyn., *14*, 225–250.

Meinen, C. S. and D. R. Watts. 2000. Vertical structure and transport on a transect across the North Atlantic Current near 42°N: Time series and mean. J. Geophys. Res., *105*, 21,869—21,892.

Merryfield, W. J., P. F. Cummins and G. Holloway. 2001. Equilibrium statistical mechanics of barotropic flow over finite topography. J. Phys. Oceanogr., *31*, 1880–1890.

Nycander J. and J. H. LaCasce. 2004. Stable and unstable vortices attached to seamounts. J. Fluid Mech., *507*, 71–94.

Qiu B. and S. Chen. 2005. Variability of the Kuroshio Extension Jet, recirculation gyre, and mesoscale eddies on decadal time scales. J. Phys. Oceanogr., *35*, 2090–2103.

Savidge, D. K. and J. M. Bane. 1999a. Cyclogenesis in the deep ocean beneath Gulf Stream 1. Description. J. Geophys. Res., *104*, 18,111–18,126.

—— 1999b. Cyclogenesis in the deep ocean beneath Gulf Stream 2. Dynamics. J. Geophys. Res., *104*, 18,127–18,140.

Shay, T. J., J. M. Bane, D. R. Watts and K. L. Tracey. 1995. Gulf Stream flow field and events near 68°W. J. Geophys. Res., *100*, 22,565–22,589.

Smith, W. H. F. and D. T. Sandwell. 1997. Global seafloor topography from satellite altimetry and ship depth soundings, Science, *277*, 1957–1962.

Sutyrin, G. G. 2006. Critical effects of a tall seamount on a drifting vortex. J. Mar. Res., *64*, 297–317.

Thompson, L. 1993. Two-layer quasigeostrophic flow over finite isolated topography. J. Phys. Oceanogr., *23*, 1297–1314.

Vallis, G. K. and M. E. Maltrud. 1993. Generation of mean flows and jets on a beta plane and over topography. J. Phys. Oceanogr., *23*, 1346–1362.

Vastano, A. C. and B. A. Warren. 1976. Perturbations to the Gulf Stream by Atlantis II Seamount. Deep-Sea Res., *23*, 681–694.

Verron, J. and C. Le Provost. 1985. A numerical study of quasi-geostrophic flow over isolated topography. J. Fluid Mech., *154*, 231–252.

Watts, D. R., C. Sun and S. Rintoul. 2001. A two-dimensional gravest empirical mode determined from hydrographic observations in the Subantarctic Front. J. Geophys. Res., *31*, 2186–2209.

Watts, D. R., K. L. Tracey, J. M. Bane and T. J. Shay. 1995. Gulf Stream path and thermocline structure near 74°W and 68°W. J. Geophys. Res., *100*, 18,291–18,312.

Received: *14 August 2008*; revised: *14 July 2009*.